Induced-Drag Characteristics of Crescent-Moon-Shaped Wings

C.P. van Dam*
University of California, Davis, California

Results are presented of a theoretical study conducted to analyze the potential drag reduction characteristics of wings with highly tapered aft-swept tips at subsonic speeds. These planar wings, also named crescent-moon-shaped wings or wings with curved planform, can produce induced drag less than the minimal value obtained with the classical unswept elliptical wing for a constant lift and wing span. The induced-drag reduction is the result of the nonplanar wing and wake shape at the angle of attack. For an example wing of aspect ratio 7, the crescent-moon shape provides a reduction in cruise induced drag of 8.0% as compared to an unswept elliptical wing.

Nomenclature

$\mathcal{R}$	$=b^2/S$, aspect ratio
b	= wing span
c	= section chord
c_{av}	$=S/b$, average wing chord
C_D, C_{D_i}	= induced-drag coefficient
c_l	= section lift coefficient
C_L	= wing lift coefficient
K_i	$=C_{D_i}/(C_{D_i})_{ell}$, induced-drag coefficient ratio for a constant C_L
N	= number of surface panels
S	= wing area
U	= freestream velocity
U_∞	= x component of freestream velocity
W_∞	= z component of freestream velocity
x, y, z	= Cartesian coordinate system variables
α	= angle of attack
η	$=y/(b/2)$, nondimensional spanwise coordinate
Λ_{LE}	= leading-edge sweep angle

Subscripts

c	= chordwise
ell	= elliptical
r	= root
s	= spanwise
t	= tip

Introduction

In nature, fast and prolonged cruising fish (e.g., tuna, swordfish, sailfish, marlin) and cetaceans (dolphins, whales) utilize crescent-moon-shaped tails having moderate-to-high aspect ratios. Also, wings of efficiently soaring sea birds and certain land birds (e.g., swift) display this characteristic planform shape. Why would nature produce this planar planform shape with backward curvature after millions of years of evolution when it is generally known that the minimum induced drag of a planar lifting surface is obtained for an elliptical spanwise load distribution that produces a constant downwash?[1]

Recently, Ashenberg and Weihs[2] analyzed the problem of minimum induced drag for wings with forward and backward curvature. Their results show that induced drag equal to but not less than the minimum value obtained for the classical straight wing with elliptical loading distribution can be achieved with planar curved planforms. In order to obtain the mimimum value of induced drag for the wing with backward sweep, it may be required to introduce a substantial amount of washout, while for the wing with forward sweep, it may be necessary to incorporate washin. The twist requirement has a severe disadvantage, however, because now the minimum induced drag is obtained only at the angle of attack for which the wing twist distribution is optimized. At off-design conditions, drag penalties are incurred and the induced drag produced by the twisted swept wing will be higher than for the untwisted unswept elliptical wing for a constant lift coefficient. This paper will demonstrate that an untwisted planar crescent-moon wing can be more efficient than an unswept elliptical wing. A computation method that correctly accounts for the influence of the trailing wake must be applied in order to obtain this somewhat unexpected result.

Zimmer[3,4] demonstrated that crescent-moon planform shapes can significantly reduce the level of induced drag produced by a wing. The results are obtained with a vortex-lattice method that models the lifting surface by its mean camber line and takes into account the nonlinear effect of the trailing vortex sheet. Consequently, the influence of airfoil thickness is assumed to be negligible and the leading-edge suction force is modeled mathematically. Zimmer's work resulted in the Dornier New Technology Wing (Dornier Do-228), which represents a practical (and somewhat compromised) application of the crescent-moon planform shape.

In this study, a nonlinear surface panel method is applied to study the drag characteristics of a crescent-moon-shaped lifting surface of aspect ratio 7. Consequently, no approximations are required to calculate the induced-drag force.

Analysis Method

Within the framework of Prandtl's classical lifting-line method,[5] the minimum induced-drag coefficient for a planar wing is $(C_{D_i})_{ell}=C_L{}^2/\pi\mathcal{R}$ and this value is obtained for an elliptical spanwise load distribution, as shown by Munk.[1] The wake of the wing is modeled as a flat trailing vortex sheet that originates at the trailing-edge separation line and the induced drag can be computed using a Trefftz-plane momentum technique. This flow model with the flat trailing wake parallel to the x axis (Fig. 1) is also applied in lifting surface theory and it is generally adequate except in the wing-tip regions where the treatment is poor. In the tip regions, vortex rollup occurs along the free edges of the trailing wake and this influences the aerodynamic loading of the

Received May 1, 1986; presented as Paper 86-1824 at the AIAA 4th Applied Aerodynamics Conference, San Diego, CA, June 9-11, 1986; revision received Nov. 10, 1986.

*Assistant Professor, Department of Mechanical Engineering, Division of Aeronautical Science and Engineering. Member AIAA.

wing. More importantly, at angle of attack, the trailing edge of a planar wing with aft-swept wing tips (or a crescent-moon-shaped wing) and the wake springing from the trailing edge are highly nonplanar. This geometric feature is not modeled by methods that assume the trailing wake to be flat and parallel to the x axis. In Fig. 2, the nonplanar shape as a consequence of the angle of attack is illustrated for an example wing. The vertical displacement of the wing-tip region is large when compared to the vertical displacement of the inboard region, demonstrating that the classical planar representation of the wing and its wake may be too simplistic for this type of configuration.

The surface panel method developed by Maskew[6] correctly accounts for these wake effects. This low-order potential flow method uses quadrilateral panels on which doublet and source singularities are distributed in a piecewise-constant manner. The strengths of the source singularities are obtained from the external Neumann boundary condition, which requires zero flow velocity normal to the surface. The strengths of the surface doublet singularities are solved after imposing the internal Dirichlet boundary condition of zero perturbation potential at the inside centers of all surface panels simultaneously. The doublet strengths of wake panels are determined by the Kutta condition at the trailing edge of the lifting surface. The wake doublet values vary in the spanwise direction, while they are constant in the streamwise direction. The method allows for wake relaxation and vortex rollup. A quickly converging iterative procedure aligns the wake panels with the local flow direction and provides for the nonlinear influence of the trailing wake.

In order to verify the method's lift-and-drag calculations, an unswept wing of $\mathcal{R}=7$ with an elliptical planform shape has been analyzed. In the chordwise direction, the NACA-0012 wing section shape is modeled using 100 panels, 50 on the upper and 50 on the lower surface. On both the lower and upper surfaces, a cosine distribution with smaller panels near the leading and trailing edges is used. In spanwise direction, 10 panels in a half-cosine distribution with smaller panels near the wing tip are used. The calculated lift and drag coefficients are listed in Table 1 for the wing at an angle of attack of 4 deg. The drag coefficient is obtained by suitable integration of the surface pressures and represents the induced-drag coefficient for the inviscid-flow model without flow separation. After two wake iterations, the solution is virtually converged and an induced-drag factor $K_i=1.0$ is calculated, as expected.[5] The calculated lift coefficient is about 1.0% greater than the lift coefficient calculated with Van Dyke's expression for the lift curve slope for elliptical wings of moderate-to-high aspect ratio.[7] This overprediction can be expected when computing wing aerodynamic characteristics with an inviscid surface panel method.[8] The spanwise load distribution for the wing is shown in Fig. 3 and compared with the elliptical load distribution.

In Figs. 4 and 5, the influence of panel density on the calculated values of C_L and C_D is shown. The straight elliptically shaped wing with its symmetrical section shape does not incorporate twist and, consequently, the inviscid method should calculate $C_L=C_D=0$ for $\alpha=0$ deg. At $\alpha=0$ deg, the maximum error in lift coefficient is very small ($C_L<0.0004$) for all cases analyzed. The error in drag coefficient is strongly dependent on chordwise panel density N_c and the results of Fig. 4 indicate $N_c=100$ is required to obtain an accurate value for C_D through integration of the surface pressures. The upper limit of the current version of the method is 1000 panels, which limits the number of panels in spanwise direction to $N_s=10$. The dependence of C_L and C_D on N_S is small and $N_S=10$ in a half-cosine distribution provides accurate values for the aerodynamic coefficients (Fig. 5). The lift and drag results in Table 1 and Fig. 3 and the following results include the zero angle-of-attack correction.

These results and other published comparisons demonstrate that the method of Ref. 6 is an excellent tool to analyze the

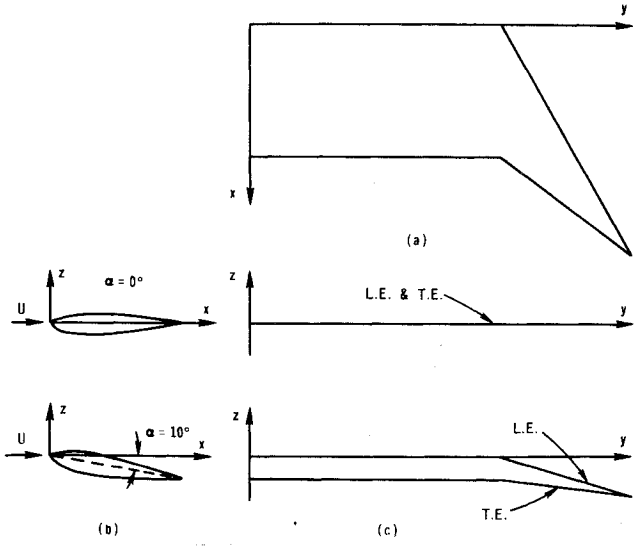

Fig. 2 Sketch of wing with aft-swept tip: a) top view; b) root chord; c) rear view displaying vertical location of leading edge (L.E.) and trailing edge (T.E.).

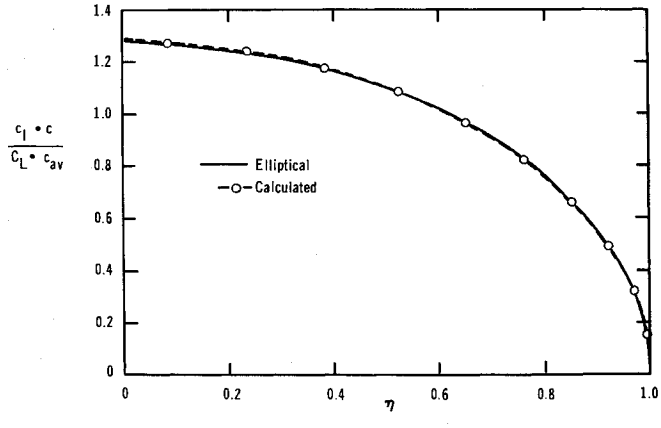

Fig. 3 Span load distribution of elliptical wing at $\alpha=4.0$ deg.

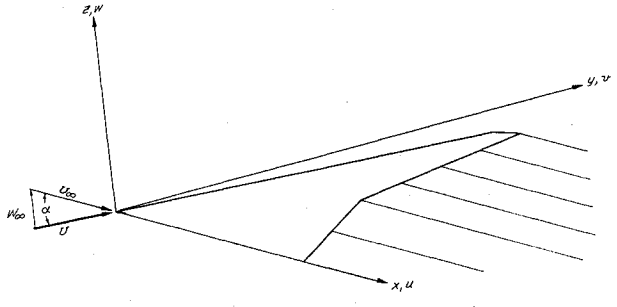

Fig. 1 Classical representation of lifting surface and its wake.

Table 1 Calculated lift and drag coefficients for an unswept wing of $\mathcal{R}=7$ with elliptical planform shape at $\alpha=4.0$ deg

Wake iteration	C_L	C_D	K_i
0	0.34288	0.00510	0.9540
1	0.34207	0.00532	0.9998
2	0.34178	0.00531	0.9997
3	0.34176	0.00531	0.9998
4	0.34173	0.00531	0.9999
5	0.34175	0.00531	0.9998

aerodynamic characteristics of a lifting surface, including the nonlinear influence of its wake.

Results and Discussion

The results are generated for a constant wing aspect ratio $\mathcal{R}=7$. The various wing configurations do not incorporate any geometric twist or dihedral. The section shape is provided by the standard NACA-0012 airfoil. The symmetrical section shape is modeled in a similar manner as the section shape of the previously described elliptical wing. In Fig. 6, six wing configurations are shown. The only difference between the six configurations is the sweep angle of the outboard wing portion. The inboard portion of the wings through $\eta=0.65$ is kept unchanged. The wing-tip region is sheared to obtain the wing-tip geometries with various sweep angles. Therefore, the chord lengths and section shapes parallel to the plane of symmetry are constant and wing span and wing area are unchanged.

The effects of the change in tip sweep angle on the wing aerodynamic characteristics are shown in Figs. 7 and 8. The main interest focuses on induced drag and a minimum value for $K_i=C_{D_i}/(C_{D_i})_{\text{ell}}$ is obtained for a wing-tip leading-edge sweep angle of 52.5 deg, as shown in Fig. 7. For this wing configuration, $K_i=1.0351$ and, thus, the induced-drag coefficient is 3.5% greater than the minimum induced drag coefficient $(C_{D_i})_{\text{ell}}$ for a given lift coefficient. Thus, an aft-swept tip planform modification does reduce the induced drag produced by a lifting surface. Its beneficial influence, however, is limited by planform characteristics of the inboard wing portion. Also, the abrupt changes in sweep angle and taper ratio produce an indentation in the spanwise load distribution and, consequently, an increase in vortex shedding at that location. The spanwise load distribution for two configurations, CONFG1 and CONFG5, are plotted in Fig. 8 and compared with the elliptical distribution. The high taper ratio in the wing-tip region produces a peak in the spanwise section lift distribution near the tip of the wing. Therefore, at high angles of attack, one might expect flow separation to occur on the highly swept tip. However, tip stall may be prevented through the application of separation-induced leading-edge vortex flow on the highly swept outboard portion of the wing in combination with a sharp leading-edge dog tooth and a drooped leading edge. The high-angle-of-attack aerodynamic characteristics of lifting surfaces with aft-swept tips are still being researched and the results will be reported elsewhere.

It can be shown that a more optimum configuration can be obtained through the introduction of taper and shear in a continuous manner as compared to the previously introduced discontinuous taper and shear angle. The wing shape can be prescribed by the following two expressions:

$$x_{\text{LE}}(\eta)=x_t(1-\sqrt{1-\eta^2}) \tag{1}$$

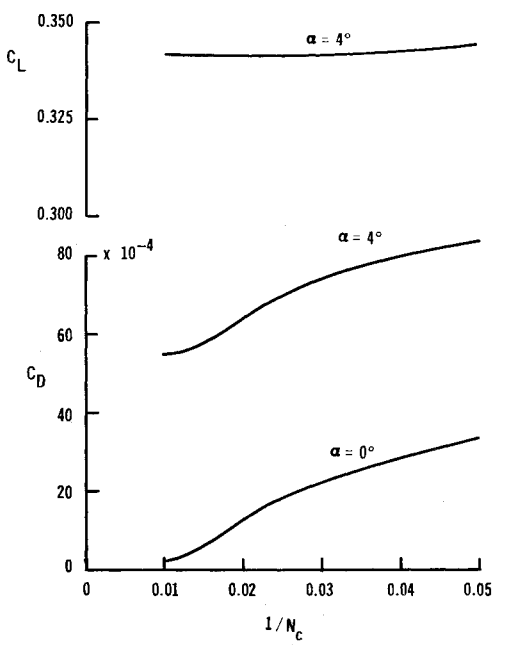

Fig. 4 Convergence of lift and drag for elliptical wing ($N_s=10$, one wake iteration).

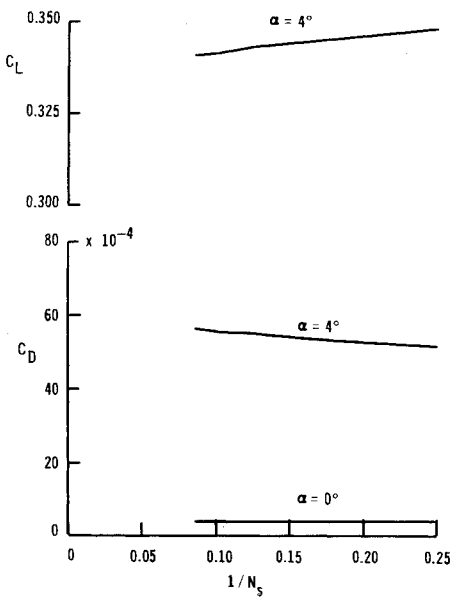

Fig. 5 Convergence of lift and drag for elliptical wing ($N_c=80$, one wake iteration).

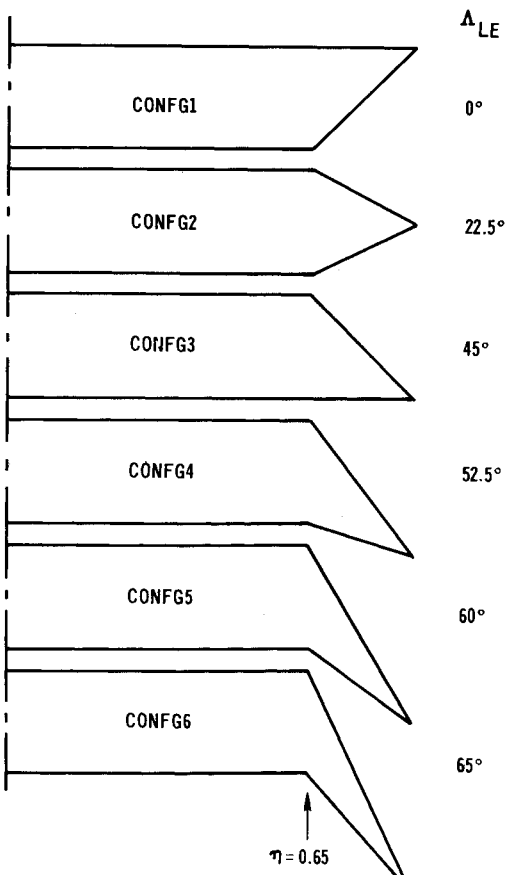

Fig. 6 Various swept-tip shaped wings of $\mathcal{R}=7$.

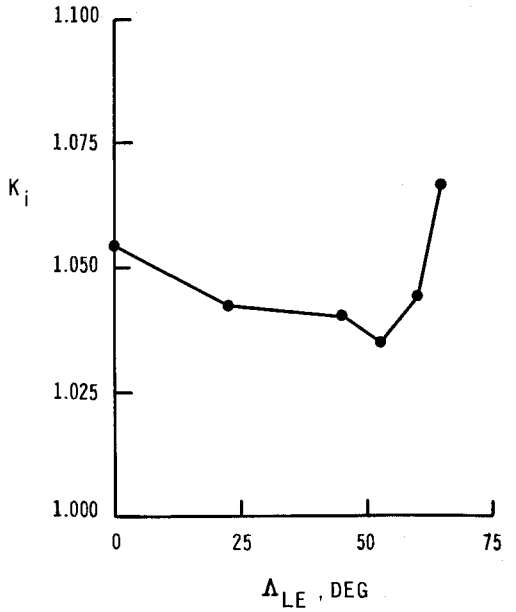

Fig. 7 Influence of wing-tip shear angle on induced drag ($\mathcal{R}=7$, $\alpha=4.0$ deg).

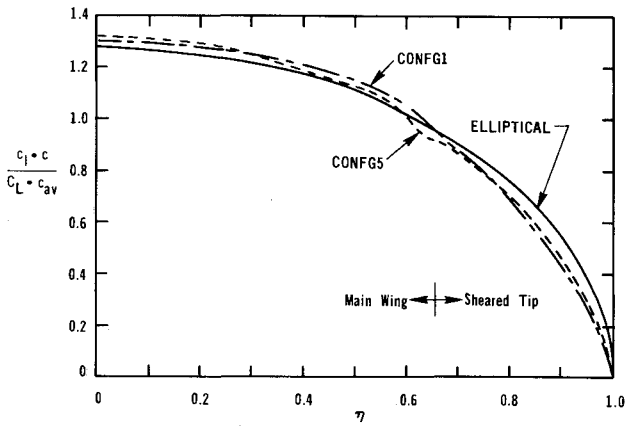

Fig. 8 Span load distributions for two wing configurations at $\alpha=4.0$ deg.

$$c(\eta)=c_r\sqrt{1-\eta^2} \tag{2}$$

Thus, the wing is so constructed that its planform is bounded by two half-ellipses with identical major axes equal to the wing span. The previously discussed elliptically shaped straight wing is obtained for $x_t=0.25$ nd $c_r=1.0$. In Fig. 9, five wing configurations for $c_r=1.0$ and $x_t=0.0$–1.5 are sketched, whereas the spanwise load distributions are shown in Fig. 10 and compared with the elliptical distribution. For a constant chord distribution, backward sweep produces an increase in aerodynamic loading outboard toward the tip, while forward sweep produces a reduction in tip loading, as expected.[2] The influence of wing-tip location x_t on induced drag is displayed as a function of wake iteration in Fig. 11. The solutions are virtually converged after two wake iterations and an induced-drag coefficient smaller than the "minimum" drag coefficient is obtained for $x_t>0.25$. It should be remembered that planform area and aspect ratio are unchanged as compared to the previous configurations. Thus, induced drag less than that obtained on a wing with an elliptical load distribution is calculated for these backward-curved wings with nonelliptical load distribution. The planform shape for $x_t=1.5$ is quite similar to the shape of lifting surfaces observed in nature.[9] This crescent-moon-shaped

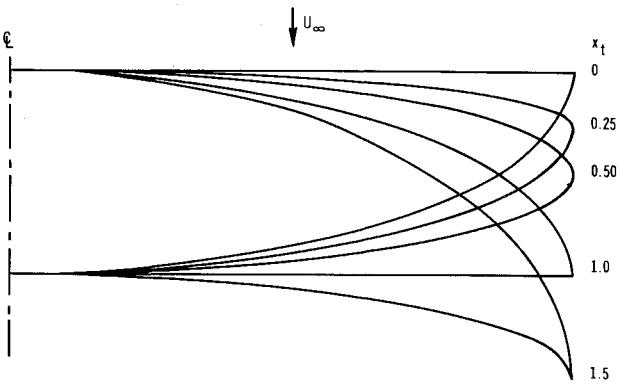

Fig. 9 Planform geometry for various elliptical wings of $\mathcal{R}=7$.

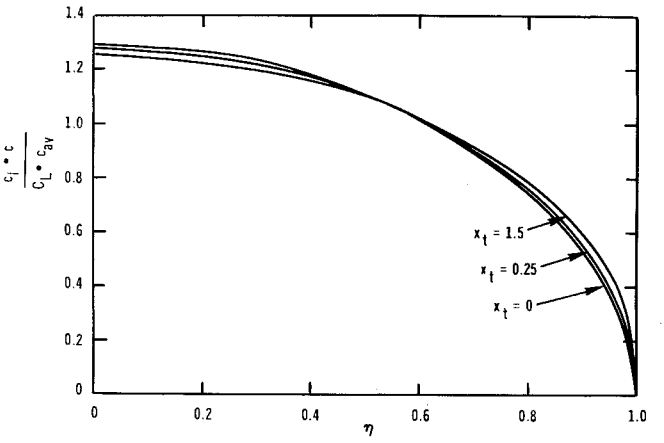

Fig. 10 Spanwise load distribution for three elliptically shaped wings ($\alpha=4.0$ deg).

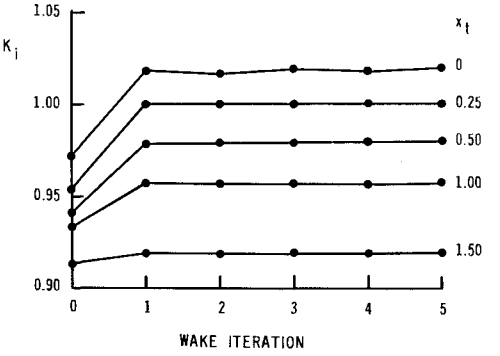

Fig. 11 Influence of wing-tip chordwise location on induced drag for elliptically shaped configurations.

wing configuration produces 8.0% less induced drag than an unswept elliptically shaped wing for a constant wing span and lift.

Throughout this study, the chordwise section shape and, thus, the panel spanwise edges have been specified in a plane parallel to the x-z plane. For swept surfaces, this paneling practice results in panels that are highly skewed instead of approximately rectangular. The influence of the somewhat undesirable skewed panel shape was investigated by modeling the elliptical wing ($x_t=1.5$) with the panel spanwise edges normal to the curved quarter-chord line. The originally calculated induced-drag ratio is (1000 panels, 5 wake iterations) $K_i=0.9190$, whereas for the wing with the more rectangular wing panels (and otherwise identical conditions) $K_i=0.9245$. Thus, modifications in the paneling scheme

slightly alter the calculated results but they do affect the overall conclusions of this study.

The planform geometry specified by Eqs. (1) and (2) should not be considered to be optimal. The geometry and spanwise load distribution of optimal planar crescent-moon-shaped lifting surfaces are still being investigated.

Conclusions

The study demonstrates that tapering and sweeping the outboard portion of a lifting surface may significantly improve its aerodynamic performance at subsonic speeds. Results obtained with a nonlinear surface panel method indicate that induced drag less than the minimal value obtained with the classical unswept wing with elliptical local distribution is achievable for planar crescent-moon-shaped wings. The induced-drag reduction is produced by the nonplanar shape due to angle of attack of the wing and its wake.

Acknowledgment

This study has been supported in part by NASA Langley Research Center.

References

[1]Munk, M.M., "The Minimum Induced Drag of Aerofoils," NACA Rept. 121, 1921.

[2]Ashenberg, J. and Weihs, D., "Minimum Induced Drag of Wings with Curved Planform," *Journal of Aircraft,* Vol. 21, Jan. 1984, pp. 89-91.

[3]Zimmer, H., "The Significance of Wing End Configuration in Airfoil Design for Civil Aviation Aircraft," NASA TM-75711, 1979.

[4]Zimmer, H., "The Aerodynamic Optimization of Wings in the Subsonic Speed Range and the Influence of the Design of the Wing Tips," Dr.-Ing. Dissertation, University of Stuttgart, FRG, June 1983.

[5]Prandtl, L., "Applications of Modern Hydrodynamics to Aeronautics," NACA Rept. 116, 1921.

[6]Maskew, B., "Prediction of Subsonic Aerodynamic Characteristics—A Case of Low-Order Panel Methods," *Journal of Aircraft,* Vol. 19, Feb. 1982, pp. 157-163.

[7]Van Dyke, M., *Perturbation Methods in Fluid Mechanics,* Parabolic Press, Stanford, CA, 1975, Note 13.

[8]Margason, R.J., Kjelgaard, S.O., Sellers, W.L., III, Morris, C.E.K., Jr., Walkey, K.B., Shields, E.W., "Subsonic Panel Methods—A Comparison of Several Production Codes," AIAA Paper 85-0280, Jan. 1985.

[9]Van Dam, C.P., "Efficiency Characteristics of Crescent-Shaped Wings and Candal Fins," *Nature,* in print.